ACS OMEGA

http://pubs.acs.org/journal/acsodf

Article

DFT Study on the Adsorption of Monomeric Hydroxyl Aluminum on Fe(II)/Mg Replacement Kaolinite (001) Surfaces

Fei Fang, Yan Zheng, Jun Chen, Chunfu Liu, and Fanfei Min*

Cite This: *ACS Omega* 2022, 7, 39662−39670

Read Online

ACCESS | Metrics & More | Article Recommendations

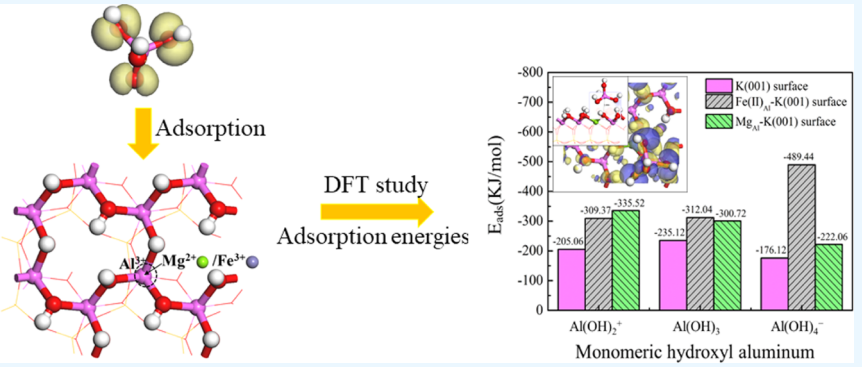

ABSTRACT: In the natural environment, Al and Si in the kaolinite crystal structure are likely to form lattice defects or be replaced by low-valence positive ions so that the base surfaces have permanent negatively charged sites. It is therefore very important to investigate the adsorption process and adsorption mechanism of adsorbates on the replaced surfaces. In this paper, two types of surface models formed by replacing Al atoms in the alumina octahedron of kaolinite (001) surface with Fe(II) and Mg were selected as the adsorption surfaces, these being the kaolinite $Fe(II)_{Al}$-(001) and Mg_{Al}-(001) surfaces, respectively. Then, we used density functional theory (DFT) to simulate the adsorption of three monomeric hydroxy aluminum models (i.e., $Al(OH)_2^+$, $Al(OH)_3$, and $Al(OH)_4^-$) on the two replaced surfaces. Results show that, when compared to the adsorption on the ideal kaolinite (001) surface, the adsorption energies of the three adsorbates adsorbed on the replaced surfaces are lower and the adsorption is more stable. When the three adsorbates are adsorbed on the kaolinite $Fe(II)_{Al}$-(001) surface, adsorption stability increases with the number of hydroxyl groups, and hydrogen bonding and electrostatic adsorption play a major role. Conversely, when they were adsorbed on the kaolinite Mg_{Al}-(001) surface, the stability of the adsorption deteriorated as the number of hydroxyl groups increased. Moreover, the decisive roles are the interaction between the aluminum atoms in the adsorbates and the oxygen atoms on the replaced surface and the electrostatic adsorption.

1. INTRODUCTION

Kaolinite is a clay mineral and its layered structure comprises a layer of −Al− (O, OH) octahedron and a layer of −Si−O tetrahedron. This layered structure is connected via hydrogen bonding.[1] Consequently, when subjected to external forces, kaolinite is more likely to split in a direction parallel to the layer and break into two different types of surfaces with different properties, i.e., base surfaces and edge surfaces. So far, to reduce research challenges that are complex for this topic, theoretical[2−9] and experimental studies[10−15] need to be continued on the ideal kaolinite structure without any lattice defects. Yet, the structure of the actual kaolinite crystal in the natural surrounding is different from that of the ideal kaolinite crystal due to the replacement of the aluminum and silicon ions by the lower positive valence ions or the formation of defects, which also leads to changes in the electrical properties of the crystal surfaces.[16,17] As part of the scientific research process, we need to understand how the structures and characteristics differ between the ideal and actual kaolinite crystal.

When the kaolinite crystal is cleaved, the base surfaces are negatively charged due to lattice defects or isomorphic substitution. For example, Al in the aluminum−oxygen octahedron is replaced by Fe(III), Fe(II), and Mg (which are abbreviated as $Fe(III)_{Al}$, $Fe(II)_{Al}$, and Mg_{Al}, respectively), while Si in the silicon−oxygen tetrahedron is replaced by

Received: May 17, 2022
Accepted: August 10, 2022
Published: October 25, 2022

Fe(III) and Al. For the base surfaces, the charge properties are independent of the solution's pH value, but they are related to the defects in the lattice and the substitution position of lower valence positive cations.[18,19] In 1954, Schofield et al.[20] placed pure kaolinite in a certain concentration of NaCl solution for shaking. The kaolinite washed with distilled water retained exchangeable Na, which indicated that the crystal was negatively charged. When the kaolinite crystals were placed in 0.5 M NaCl solution and reshaken, they would adsorb chloride, which confirmed that parts of the kaolinite crystal's surfaces (presumably the edge surfaces) were positively charged. Malden et al.[21] confirmed the substitution of aluminum by trivalent iron ions in the aluminum−oxygen octahedron of kaolinite in 1967. Mestdagh et al.[22] and Balan et al.[23] studied the relationship between kaolinite crystallinity and iron content and the substitution sites using electron paramagnetic resonance (EPR).

With the development of quantum chemistry calculations, scholars also began to analyze the lattice defects of the kaolinite crystal from the perspective of theoretical simulation. Chi et al.[24] showed that the permanent negative charge generated by Al substitution of Si in the silicon−oxygen tetrahedral of kaolinite is not significant. In 2009, through the theoretical calculation with density functional theory (DFT), He et al.[25] demonstrated that Fe in the natural environment could be easily substituted for Al atoms in aluminum oxide octahedron, and the substitution of Mg for Al also introduced a negative charge in the kaolinite crystal structure. Then, in 2012, the team further studied the adsorption and penetration of H_2O on the kaolinite (001) surface with Mg, Ca, and Fe(II) doping through DFT theoretical calculations.[26] Recently, Liu et al.[27] calculated that the content order of differently coordinated Fe in kaolinite in a certain area and the degree of ease of substitution are six coordination Fe^{2+} $(Fe(II)_{Al})$ > four coordination Fe^{3+} $(Fe(III)_{Si})$ > six coordination Fe^{3+} $(Fe(III)_{Al})$ using DFT theoretical simulation. Additionally, the test results by a Mössbauer spectrometer were consistent with the simulation outcomes. Chen et al.[28] calculated through theoretical simulation that the lattice substitution of Fe mainly improved the reactivity of the kaolinite (001) surface. The above description shows that the actual kaolinite crystal structure and surface characteristics have been changed. Subsequently, it is of practical significance to examine the adsorption mechanism of adsorbate on the replaced and defective kaolinite surfaces.

Kaolinite is one of the main components of clay minerals in mineral processing wastewater. Aluminum salt, as a common inorganic salt coagulant, is often used in the treatment of mining wastewater to accelerate its settlement. In the solution environment of mineral processing wastewater (pH = 7−9), aluminum ions often exist as monomers, namely, $Al(OH)_2^+$, $Al(OH)_3$, and $Al(OH)_4^-$. In this paper, we constructed two structural models of Al in the alumina octahedron of the kaolinite (001) surface replaced by Fe(II) and Mg. The DFT simulation served to calculate the stable adsorption configurations of the three monomer hydrolysis components of aluminum salts on the two types of replaced kaolinite surfaces. Meanwhile, we analyzed the adsorption mechanism and adsorption difference of the three adsorbates on different replaced surfaces from the aspects of bonding formation, charge transfer, and density of states. This research can also provide a theoretical basis for the development and design of aluminum-containing reagents and the optimization of the reagent system.

2. COMPUTATIONAL METHODS AND MODELS

2.1. Computational Methods. The construction of models and all simulation calculations were done using Materials Studio 2017 (Accelrys, Inc.). The optimization and property calculation of the adsorption models are mainly carried out using the CASTEP module based on DFT.[29]

With reference to the necessary parameters, the ultrasoft pseudopotential (USPP) was selected, and the energy cutoff for the plane waves was 460 eV.[30] For the convergence tolerance scenario, we chose fine as the self-consistent iterative convergence accuracy. The corresponding relevant parameters were 1.0×10^{-5} eV/atom for total energy, 0.03 eV/Å for maximum atomic force, 0.05 GPa for maximum atomic stress, and 1×10^{-4} nm for maximum atomic displacement. The exchange-correlation function was set to GGA-PBE (abbreviation of Generalized Gradient Approximation with Perdew−Burke−Ernzerhof).[31] For electronic structure calculations, the spin polarization method was used, with the spin parameter set to +4 for the Fe(II) atom. Furthermore, we chose TS (abbreviation for the Tkatchenko−Scheffler method) to correct the dispersion force in the optional parameters.[32] The grid parameters about k-points of the kaolinite supercell models and the surface models were selected as $(4 \times 2 \times 3)$ and $(2 \times 2 \times 1)$, respectively. Meanwhile, $Al(OH)_2^+$, $Al(OH)_3$, and $Al(OH)_4^-$ were optimized in a 15 Å × 15 Å × 15 Å cubic box and the *k*-point was set to γ. The other optimization parameters were the same as the kaolinite supercell models. When calculating the adsorption of adsorbate on the kaolinite replaced surfaces, the parameter settings were the same as those in the surface model, except that the *k*-point was set to γ.

All simulation calculations were carried out in the reciprocal space, and the calculation of the pseudopotential of the atoms involved in the calculation selects the valence electrons as Al $3s^23p^1$, Si $3s^23p^2$, Fe $3d^64s^2$, Mg $2p^63s^2$, O $2s^22p^4$, Na $2p^63s^1$, and H $1s^1$.

2.2. Kaolinite Surface Models. In our work, the supercells of the calculation models were obtained by Fe(II) and Mg atoms replacing the Al atoms in the kaolinite $(2 \times 1 \times 1)$ supercell models, which were called $Fe(II)_{Al}$-K and Mg_{Al}-K, respectively. During the replacement process, the resulting charge loss was compensated by adding a Na^+ ion. To investigate the difficulty of replacing Al with Fe(II) and Mg atoms, we performed lattice substitution energy calculations on the two supercells after replacement, and the calculation formula is as follows:[33]

$$E_f = E_{impurity}^{total} + \mu_\chi - E_{ideal}^{total} - \mu_{impurity}$$

where $E_{impurity}^{total}$ is the total energy of kaolinite crystal after replacement, E_{ideal}^{total} is the total energy of the ideal kaolinite crystal, and μ_χ and $\mu_{impurity}$ are the chemical potentials of the replaced atom and impurity atom, respectively. The balance ion (Na^+) is not considered here.

The surface models used in the calculations were cut from the $Fe(II)_{Al}$-K and Mg_{Al}-K supercell models along the (001) direction, which were modeled by a slab made up of six atomic layers and with a vacuum thickness of 20 Å. The Fe(II) and Al(OH)- and Mg and Al(OH)-terminated surfaces were called the kaolinite $Fe(II)_{Al}$-(001) and Mg_{Al}-(001) surfaces and abbreviated as $Fe(II)_{Al}$-K(001) and Mg_{Al}-K(001) surfaces in

https://doi.org/10.1021/acsomega.2c03087
ACS Omega 2022, 7, 39662−39670

Table 1. Characteristics of Unit Cells and Calculation of Lattice Substitution Energy

	lattice parameters (Å)			cell angel (°)					
models	*a*	*b*	c	*α*	*β*	*γ*	volume (Å^3)	energy (eV)	E_f (eV)
ideal-K	5.180	8.971	7.358	92.280	105.593	90.054	329.063	−8686.517	
$Fe(II)_{Al}$-K	5.188	8.957	7.579	91.876	105.472	90.510	339.225	−9490.110	3.572
Mg_{Al}-K	5.215	9.078	7.407	92.320	105.448	89.860	337.312	−9600.164	6.021
Exp.[35]	5.153	8.942	7.391	91.926	105.046	89.797	329.910		

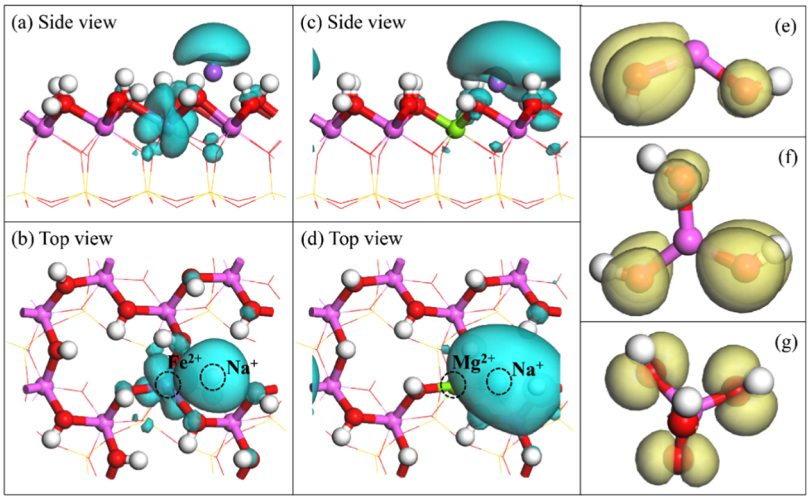

Figure 1. LUMO distributions of the replaced surfaces models ((a, b) $Fe(II)_{Al}$-K(001) surface and (c, d) Mg_{Al}-K(001) surface). HOMO distributions of the adsorbates models ((e) $Al(OH)_2^+$, (f) $Al(OH)_3$, and (g) $Al(OH)_4^-$). The isovalue is 0.03 electrons/Å^3.(H O Al Si Fe Mg Na)

the tables below, respectively. During the geometric optimization process, the upper four sublayers were relaxed, and the remaining sublayers at the bottom of the slab were fixed.[34] The optimized parameters of the ideal kaolinite unit were close to the experimental test values[35] with a error within 1.5%, and the calculation results of the parameters were a = 5.180 Å, b = 8.971 Å, c = 7.358 Å, α = 92.280°, β = 105.593°, γ = 90.054°, and V = 329.063 Å^3.

2.3. Calculation of Adsorption Energy. The lower the adsorption energy, the more stable the adsorption of the corresponding adsorbate. The calculation formula of adsorption energy is written below

$$E_{ads} = E_{total} + E_{surface} - E_{adsorbate}$$

where E_{total} is the energy value of the adsorption configuration after the adsorbate is adsorbed on the replaced kaolinite surface, kJ/mol. $E_{surface}$ and $E_{adsorbate}$ are the energy values of the surface model and adsorbate before adsorption, kJ/mol, respectively. The adsorption energy values of the optimal adsorption configurations for $Al(OH)_2^+$, $Al(OH)_3$, and $Al(OH)_4^-$ on the ideal kaolinite (001),[30] $Fe(II)_{Al}$-(001), and Mg_{Al}-(001) surfaces are shown in Figure 2.

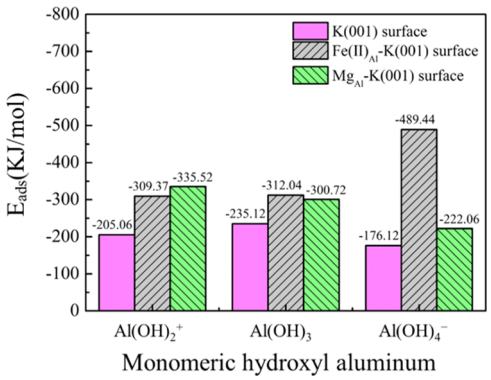

Figure 2. Adsorption energies of $Al(OH)_2^+$, $Al(OH)_3$, and $Al(OH)_4^-$ on the kaolinite (001) (Fang et al., 2020), $Fe(II)_{Al}$-(001), and Mg_{Al}-(001) surfaces.

3. RESULTS AND DISCUSSION

3.1. Surface Properties and Adsorption Characteristics. *3.1.1. Unit Cell Characteristics.* First, the CASTEP module was used to optimize the unit cells after lattice substitution, and the optimized unit cell parameters are shown in Table 1. Then, we calculated the lattice substitution energies of the unit cells replaced by Fe(II) and Mg atoms, which were 3.572 and 6.021 eV, respectively. Low lattice substitution energy corresponds to easy substitution. This shows that compared with the replacement of Al by Mg atom, Al is more easily replaced by Fe(II) atom.

3.1.2. Frontier Orbital. Up to now, the frontier orbitals theory proposed by Fukui[36,37] has been widely used in the fields of organic/inorganic chemistry, catalytic, quantum biology, and surface adsorption, which can better explain the reaction mechanism between molecules.[38] Generally speaking, the interaction of two substances is more likely to occur between the highest occupied molecular orbital (HOMO) of one substance and the lowest occupied molecular orbital (LUMO) of another substance.[39] Therefore, we can determine the possible initial adsorption sites according to the frontier orbitals theory and the structural characteristics of the replaced surface models. The purpose of this is to reduce the number of

https://doi.org/10.1021/acsomega.2c03087
ACS Omega 2022, 7, 39662−39670

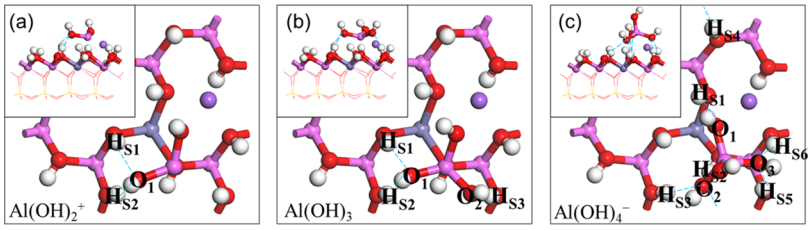

Figure 3. Stable adsorption configurations of $Al(OH)_2^+$, $Al(OH)_3$, and $Al(OH)_4^-$ on the kaolinite $Fe(II)_{Al}$-(001) surface.

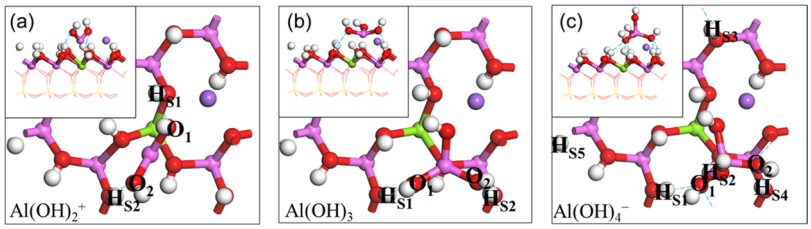

Figure 4. Stable adsorption configurations of $Al(OH)_2^+$, $Al(OH)_3$, and $Al(OH)_4^-$ on the kaolinite Mg_{Al}-(001) surface.

Table 2. Bonding Analysis of $Al(OH)_2^+$, $Al(OH)_3$, and $Al(OH)_4^-$ on the Kaolinite $Fe(II)_{Al}$-(001) and Mg_{Al}-(001) Surfaces

name	bond	population	length (Å)
$Al(OH)_2^+$ on $Fe(II)_{Al}$-K(001) surface	$O_1\cdots H_{S1}$	0.02	2.3779
	$O_1\cdots H_{S2}$	0.08	1.8498
$Al(OH)_3$ on $Fe(II)_{Al}$-K(001) surface	$O_1\cdots H_{S1}$	0.03	2.5664
	$O_1\cdots H_{S2}$	0.06	1.9916
	$O_2\cdots H_{S3}$	0.09	1.7939
$Al(OH)_4^-$ on $Fe(II)_{Al}$-K(001) surface	$O_1\cdots H_{S1}$	0.01	2.3546
	$O_2\cdots H_{S2}$	0.05	1.7760
	$O_2\cdots H_{S3}$	0.03	2.2376
	$O_2\cdots H_{S4}$	0.06	2.0227
	$O_3\cdots H_{S5}$	0.07	1.9185
	$O_3\cdots H_{S6}$	0.07	1.8773
$Al(OH)_2^+$ on Mg_{Al}-K(001) surface	$O_1\cdots H_{S1}$	0.00	2.2469
	$O_2\cdots H_{S2}$	0.07	1.8018
$Al(OH)_3$ on Mg_{Al}-K(001) surface	$O_1\cdots H_{S1}$	0.06	1.9988
	$O_2\cdots H_{S2}$	0.09	1.7327
$Al(OH)_4^-$ on Mg_{Al}-K(001) surface	$O_1\cdots H_{S1}$	0.06	1.9044
	$O_1\cdots H_{S2}$	0.04	2.1818
	$O_1\cdots H_{S3}$	0.08	1.8820
	$O_2\cdots H_{S4}$	0.07	1.9447
	$O_2\cdots H_{S5}$	0.00	2.1555

theoretical simulation calculations and to find the optimal adsorption sites more efficiently.

When $Al(OH)_2^+$, $Al(OH)_3$, and $Al(OH)_4^-$ are adsorbed on the kaolinite $Fe(II)_{Al}$-(001) and Mg_{Al}-(001) surfaces, the HOMO orbitals of the adsorbates interact with the LUMO orbitals of the replaced surfaces. Figure 1 shows the model structures of adsorbates and replaced surfaces and their corresponding diagrams of HOMO and LUMO orbitals. As shown in Figure 1a,b, the LUMO orbitals of the kaolinite $Fe(II)_{Al}$-(001) surface are mainly distributed on the balance ion Na^+ and the Fe(II) atom and the O_{Sn} atoms of the surrounding hydroxyl groups. The LUMO orbitals of the kaolinite Mg_{Al}-(001) surface are mainly distributed on the O_{Sn} atoms of the hydroxyl group near the substitution atom Mg, and the balance ion Na^+ are shown in Figure 1c,d. According to Figure 1e−g, it is found that the HOMO orbitals of the three types of hydroxyl aluminum are mainly located on the end O atoms.

3.1.3. Adsorption Energy. As can be seen from Figure 2, unlike the adsorption on the ideal kaolinite (001) surface, the monomer-hydrolyzed components of aluminum salt have different adsorption stabilities on the kaolinite (001) surface when replaced by Fe(II) and Mg. The adsorption energies of the adsorbates on the kaolinite $Fe(II)_{Al}$-(001) surface are −309.37, −312.04, and −489.44 kJ/mol, while the corresponding adsorption stability order is $Al(OH)_4^-$ > $Al(OH)_3$ > $Al(OH)_2^+$. When they are adsorbed on the kaolinite Mg_{Al}-(001) surface, the adsorption energies are −335.52, −300.72, and −222.06 kJ/mol, and the order of adsorption stability is $Al(OH)_2^+$ > $Al(OH)_3$ > $Al(OH)_4^-$. It is exactly the opposite in the case of the former. The results show that when the three monomer-hydrolyzed components adsorbed on the kaolinite (001) surfaces are replaced by Fe(II) and Mg, the adsorption energies are lower and the adsorptions are more stable than

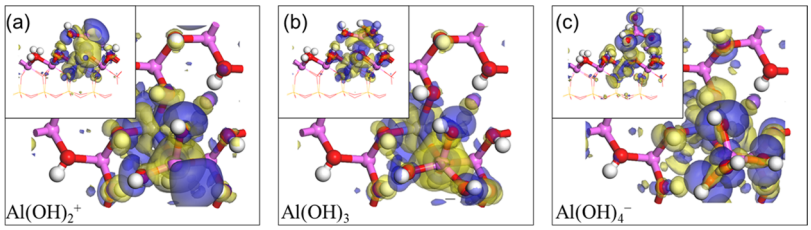

Figure 5. Differences in the electron densities of $Al(OH)_2^+$, $Al(OH)_3$, and $Al(OH)_4^-$ adsorbed on the kaolinite $Fe(II)_{Al}$-(001) surface. The isovalue is 0.01 electrons/Å^3.

https://doi.org/10.1021/acsomega.2c03087
ACS Omega 2022, 7, 39662−39670

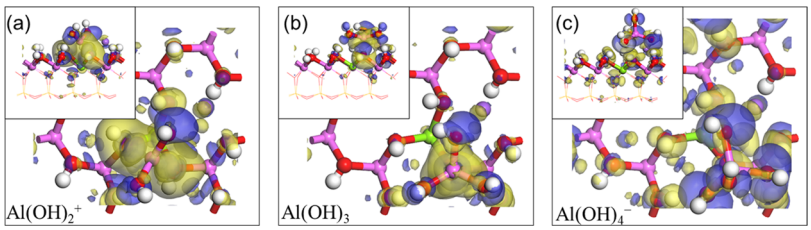

Figure 6. Differences in the electron densities of $Al(OH)_2^+$, $Al(OH)_3$, and $Al(OH)_4^-$ adsorbed on the kaolinite Mg_{Al}-(001) surface. The isovalue is 0.01 electrons/Å^3.

Table 3. Atomic Population/Charge of $Al(OH)_2^+$, $Al(OH)_3$, and $Al(OH)_4^-$ before and after Adsorption on the Kaolinite $Fe(II)_{Al}$-(001) Surface and Change in the Charges of Adsorbates and Replaced Surfaces

		before				after			
model	name	s	p	total	charge/e	s	p	total	charge/e
$Al(OH)_2^+$ on $Fe(II)_{Al}$-K(001) surface	H_{S1}	0.58	0.00	0.58	0.42	0.58	0.00	0.58	0.42
	H_{S2}	0.57	0.00	0.57	0.43	0.56	0.00	0.56	0.44
	O_1	1.88	5.28	7.16	−1.16	1.87	5.23	7.10	−1.10
	$Al(OH)_2^+$				0				−0.05
	$Fe(II)_{Al}$-K(001)				0				+0.05
$Al(OH)_3$ on $Fe(II)_{Al}$-K(001) surface	H_{S1}	0.58	0.00	0.58	0.42	0.58	0.00	0.58	0.42
	H_{S2}	0.57	0.00	0.57	0.43	0.56	0.00	0.56	0.44
	H_{S3}	0.57	0.00	0.57	0.43	0.59	0.00	0.59	0.41
	O_1	1.87	5.30	7.18	−1.18	1.87	5.25	7.12	−1.12
	O_2	1.88	5.31	7.18	−1.18	1.87	5.25	7.12	−1.12
	$Al(OH)_3$				0				−0.05
	$Fe(II)_{Al}$-K(001)				0				+0.05
$Al(OH)_4^-$ on $Fe(II)_{Al}$-K(001) surface	H_{S1}	0.62	0.00	0.62	0.38	0.60	0.00	0.60	0.37
	H_{S2}	0.60	0.00	0.60	0.40	0.60	0.00	0.60	0.42
	H_{S3}	0.57	0.00	0.57	0.43	0.56	0.00	0.56	0.43
	H_{S4}	0.57	0.00	0.57	0.43	0.57	0.00	0.57	0.43
	H_{S5}	0.57	0.00	0.57	0.43	0.57	0.00	0.57	0.41
	H_{S6}	0.61	0.00	0.61	0.39	0.63	0.00	0.63	0.44
	O_1	1.89	5.14	7.03	−1.03	1.88	5.23	7.11	−1.11
	O_2	1.89	5.11	7.00	−1.00	1.87	5.25	7.12	−1.12
	O_3	1.89	5.12	7.01	−1.01	1.87	5.24	7.11	−1.11
	$Al(OH)_4^-$				0				−0.77
	$Fe(II)_{Al}$-K(001)				0				+0.77

that on the ideal kaolinite (001) surface. When the adsorbates are adsorbed on the kaolinite $Fe(II)_{Al}$-(001) surface, the adsorption energy decreases when the number of hydroxyl groups increases. In other words, the stability of adsorption increases with the increasing number of hydroxyl groups. In contrast, when they are adsorbed on the kaolinite Mg_{Al}-(001) surface, the stability of the adsorption is weakened as the number of hydroxyl groups is increased.

3.2. Analysis of Adsorption Configuration and Bonding. Figures 3 and 4 show the stable adsorption configurations of $Al(OH)_2^+$, $Al(OH)_3$, and $Al(OH)_4^-$ adsorbed on the kaolinite $Fe(II)_{Al}$-(001) and Mg_{Al}-(001) surfaces, respectively. The Mulliken bond population and the length of the bonded atoms between the adsorbates and the replaced kaolinite surfaces are shown in Table 2. In the figures and tables below, O_n and H_{Sn} represent the oxygen atoms and hydrogen atoms, which form a hydrogen bond between the adsorbate and the replaced surface, respectively.

As shown in Figure 3, when $Al(OH)_2^+$ is adsorbed on the kaolinite $Fe(II)_{Al}$-(001) surface, two hydrogen bonds are formed between the O_n and the replaced surface H_{Sn} atoms. The maximum population value is 0.08 and the hydrogen bond strength is strong (Figure 3a). When $Al(OH)_3$ is adsorbed, three hydrogen bonds are formed, and the distribution of population value is uniform, with a maximum of 0.09 (Figure 3b). Six hydrogen bonds are formed after the adsorption of $Al(OH)_4^-$, and the maximum population value is 0.07 (Figure 3c). From the point of view of stable adsorption configurations, all three adsorbates are easy to adsorb above the oxygen atoms in the hydroxyl group parallel to the replaced surface. However, when adsorbed on the oxygen atom near Fe(II) replacement, the adsorption energy is lower and the adsorption is more stable. After adsorption occurs, the oxygen atoms in the three adsorbates form a variety of hydrogen bonds with the hydrogen atoms on the replaced surface, and these hydrogen bonds retain noticeable strength.

As can be seen from Figure 4, when $Al(OH)_2^+$ is adsorbed on the kaolinite Mg_{Al}-(001) surface, two hydrogen bonds are formed, with the population values of 0 and 0.07 (Figure 4a). When $Al(OH)_3$ is adsorbed, two hydrogen bonds are formed, with the bond population values of 0.06 and 0.09, confirming the strength of the hydrogen bonds (Figure 4b). Five hydrogen bonds are formed after the adsorption of $Al(OH)_4^-$, with the maximum population value of 0.08 (Figure 4c). The number of hydrogen bonds formed is the highest, and these hydrogen bonds are strong when $Al(OH)_4^-$ is adsorbed; however, the

https://doi.org/10.1021/acsomega.2c03087
ACS Omega 2022, 7, 39662−39670

Table 4. Atomic Population/Charge of $Al(OH)_2^+$, $Al(OH)_3$, and $Al(OH)_4^-$ before and after Adsorption on the Kaolinite Mg_{Al}-(001) Surface and Change in the Charges of Adsorbates and Replaced Surfaces

		before				after			
model	name	s	p	total	charge/e	s	p	total	charge/e
$Al(OH)_2^+$ on Mg_{Al}-K(001) surface	H_{S1}	0.63	0.00	0.63	0.37	0.64	0.00	0.64	0.36
	H_{S2}	0.54	0.00	0.54	0.46	0.57	0.00	0.57	0.43
	O_1	1.89	5.26	7.14	−1.14	1.87	5.22	7.09	−1.09
	O_2	1.88	5.28	7.16	−1.16	1.88	5.26	7.12	−1.12
	$Al(OH)_2^+$				0				+0.50
	Mg_{Al}-K(001)				0				−0.50
$Al(OH)_3$ on Mg_{Al}-K(001) surface	H_{S1}	0.54	0.00	0.54	0.46	0.56	0.00	0.56	0.44
	H_{S2}	0.58	0.00	0.58	0.42	0.59	0.00	0.59	0.41
	O_1	1.88	5.30	7.18	−1.18	1.87	5.26	7.12	−1.12
	O_2	1.87	5.31	7.18	−1.18	1.86	5.26	7.12	−1.12
	$Al(OH)_3$				0				−0.07
	Mg_{Al}-K(001)				0				+0.07
$Al(OH)_4^-$ on Mg_{Al}-K(001) surface	H_{S1}	0.54	0.00	0.54	0.46	0.55	0.00	0.55	0.45
	H_{S2}	0.59	0.00	0.59	0.41	0.61	0.00	0.61	0.39
	H_{S3}	0.57	0.00	0.57	0.43	0.57	0.00	0.57	0.43
	H_{S4}	0.58	0.00	0.58	0.42	0.58	0.00	0.58	0.42
	H_{S5}	0.62	0.00	0.62	0.38	0.62	0.00	0.62	0.38
	O_1	1.89	5.11	7.00	−1.00	1.88	5.22	7.10	−1.10
	O_2	1.89	5.12	7.01	−1.01	1.88	5.22	7.09	−1.09
	$Al(OH)_4^-$				0				−0.70
	Mg_{Al}-K(001)				0				+0.70

adsorption energy is the highest (E_{ads} = −222.06 kJ/mol), indicating that the adsorption is relatively unstable. The number of hydrogen bonds formed by the adsorption of $Al(OH)_2^+$ on the kaolinite Mg_{Al}-(001) surface is small and with poor strength; however, it has the lowest adsorption energy (E_{ads} = −335.52 kJ/mol) and the most stable adsorption. This shows that during the adsorption process, in addition to hydrogen bonding, there are other nonhydrogen bonding effects for the first two types of adsorption.

3.3. Charge Analysis. To expose the nonhydrogen bond effects between the adsorbates and the replaced surface that were analyzed in the previous section and to observe the charge transfer between the adsorbates and the replaced surface, we conducted an electron density difference analysis of the optimal adsorption configurations (Figures 5 and 6). In these figures, blue and yellow areas indicate an increase and decrease in electron density, respectively. Tables 3 and 4 show the bonded atoms' population and charge of $Al(OH)_2^+$, $Al(OH)_3$, and $Al(OH)_4^-$ before and after adsorption on the replaced kaolinite surfaces and the changes in the charge of the adsorbates and the replaced surfaces.

According to Tables 3 and 4, the hydrogen atoms participating in the bond formation exhibit electron loss, while the oxygen atoms acquire electrons. As shown in Figures 5 and 6, the electron density around oxygen atoms in the adsorbates involved in bonding increases, and the electron density around hydrogen atoms decreases on the replaced surfaces. These findings correspond to the results documented in the tables.

As shown in Table 3, when $Al(OH)_2^+$, $Al(OH)_3$, and $Al(OH)_4^-$ are adsorbed on the kaolinite $Fe(II)_{Al}$-(001) surface, the replaced surfaces transfer 0.05 e, 0.05 e, and 0.77 e, respectively, to the ions. Compared with the first two adsorbates, when the $Al(OH)_4^-$ ion is adsorbed, it has a strong electrostatic attraction to the replaced surface.

As shown in Table 3, when $Al(OH)_2^+$, $Al(OH)_3$, and $Al(OH)_4^-$ adsorbed on the kaolinite $Fe(II)_{Al}$-(001) surface, the replaced surfaces transfer 0.05 e, 0.05 e, and 0.77 e, respectively, to the ions. Compared with the first two adsorbates, when the $Al(OH)_4^-$ ion is adsorbed, it has a strong electrostatic attraction to the replaced surface.

Table 4 shows that after the $Al(OH)_2^+$ ion is adsorbed on the kaolinite Mg_{Al}-(001) surface, the ion transfers 0.50 e to the replaced surface. When the $Al(OH)_3$ molecule is adsorbed, the replaced surface transfers 0.07 e to the molecule. Following the adsorption of $Al(OH)_4^-$ ion, the replaced surface transfers 0.70 e to the ion.

It can also be seen from Figures 5 and 6 that when $Al(OH)_2^+$ and $Al(OH)_3$ are adsorbed on the kaolinite replaced surface, a large amount of electron transfer occurs between the aluminum atoms in the adsorbates and the oxygen atoms on the replaced surface. However, this charge transfer is not obvious after the adsorption of the $Al(OH)_4^-$ ion. These will be analyzed by the density of states in Section 3.4.

3.4. Partial Density of States (PDOS). To further explore the interaction between Al atoms in the adsorbates and O atoms on the surfaces when $Al(OH)_2^+$, $Al(OH)_3$, and $Al(OH)_4^-$ are adsorbed on the replaced kaolinite surfaces, we analyzed the change in the partial density of states (PDOS) before and after the adsorption of the two types of atoms (Figures 7 and 8). The Fermi level (E_f) value was set at 0 eV.

Figure 7 shows the change in the PDOS before and after the three adsorbates were adsorbed on the kaolinite $Fe(II)_{Al}$-(001) surface. When $Al(OH)_2^+$ is adsorbed, the bonding of Al 3p and O_S 2p is in the −10.3 to −2.5 eV range, and the antibonding is in the 1.5−14.0 eV range (Figure 7a). When $Al(OH)_3$ is adsorbed, the bonding of Al 3p and O_S 2p occurs in the −11.2 to −3.5 eV range, and the antibonding is in the 1.3−13.3 eV range (Figure 7b). After the adsorption of $Al(OH)_4^-$, the bonding of Al 3p and O_S 2p is in the −9.5 to −1.3 eV range,

https://doi.org/10.1021/acsomega.2c03087
ACS Omega 2022, 7, 39662−39670

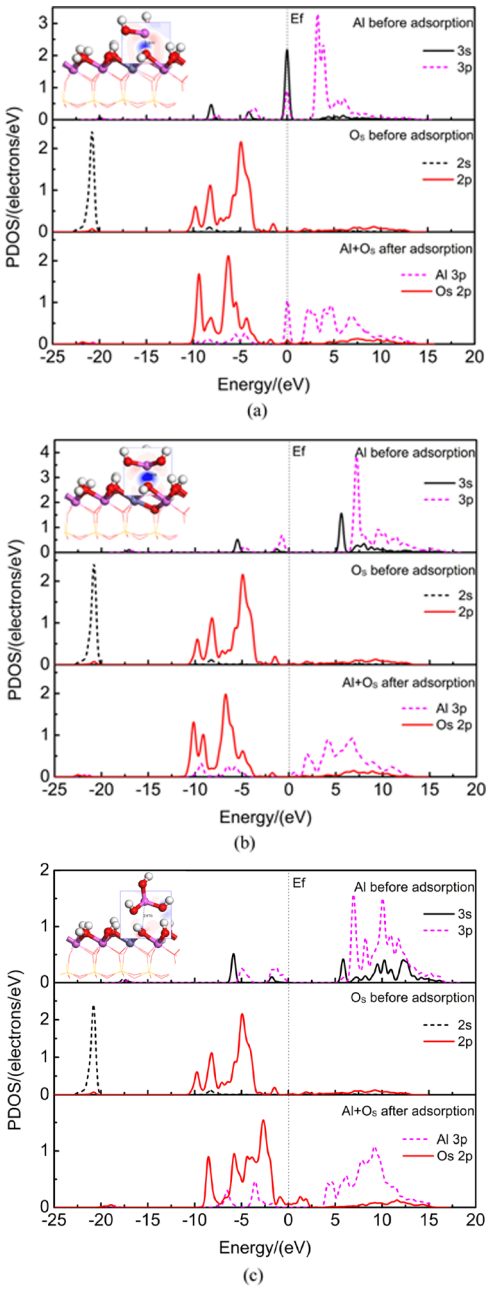

Figure 7. PDOS of Al−O_S atoms before and after the adsorbates' adsorption on the kaolinite $Fe(II)_{Al}$-(001) surface ((a) $Al(OH)_2^+$, (b) $Al(OH)_3$, and (c) $Al(OH)_4^-$).

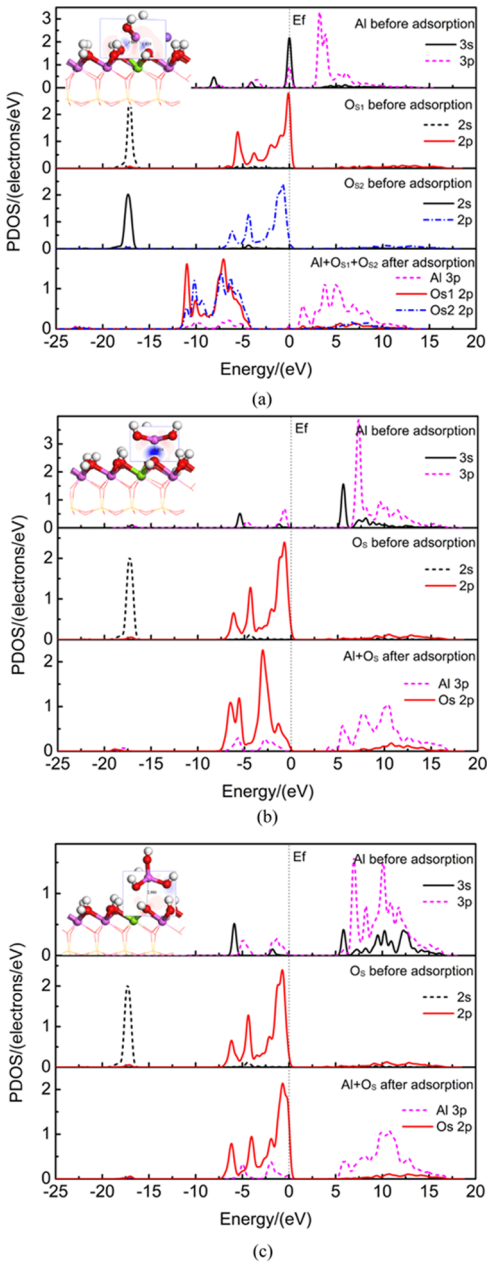

Figure 8. PDOS of Al−O_S atoms before and after the adsorbates' adsorption on the kaolinite Mg_{Al}-(001) surface ((a) $Al(OH)_2^+$, (b) $Al(OH)_3$, and (c) $Al(OH)_4^-$).

and the antibonding is in the 3.5−15.5 eV range. The bonding effect is stronger than the antibonding effect.

As shown in Figure 8, what is significant is the change in the PDOS before and after the three adsorbates were adsorbed on the kaolinite Mg_{Al}-(001) surface. When $Al(OH)_2^+$ is adsorbed, Al 3p in the adsorbate has a bonding effect with the replaced surface O_{S1} 2p and O_{S2} 2p in the −11.5 to −4.0 eV range, while the antibonding is in the 0.7−13.0 eV range. After the adsorption of $Al(OH)_3$, the bonding of Al 3p and O_S 2p occurs in the −7.5 to 0 eV range, and the antibonding is in the 5.0−16.8 eV range. When $Al(OH)_4^-$ is adsorbed, the bonding of Al 3p and O_S 2p is in the −7.5 eV to 0 eV range, and the antibonding is in the 5.0−17.0 eV range. Compared with the antibonding effect, the bonding effect is stronger.

Combined with the PDOS diagrams, it can be observed that all of the densities of states move to a lower energy level as a whole, and the density of states near the Fermi level declined after the Al−O_S atom interaction, indicating that the surface energy decreases after adsorption. In addition, the bonds between Al and O_S atoms are strong, which means that there is a strong interaction between the aluminum atoms in the adsorbates and the oxygen atoms on the replaced surfaces, and this effect wields a decisive influence on the adsorption results. When $Al(OH)_2^+$ is adsorbed on the kaolinite Mg_{Al}-(001) surface, the bonding between the Al atom and the two O_S atoms is very strong. Therefore, when $Al(OH)_2^+$ is adsorbed on the kaolinite Mg_{Al}-(001) surface, the adsorption energy is the lowest (E_{ads} = −335.52 kJ/mol) and the adsorption is the most stable.

https://doi.org/10.1021/acsomega.2c03087
ACS Omega 2022, 7, 39662−39670

4. CONCLUSIONS

(1) Compared with the replacement of Al by Mg atom, Al is more easily replaced by Fe(II) atom in the kaolinite crystals. When $Al(OH)_2^+$, $Al(OH)_3$, and $Al(OH)_4^-$ are adsorbed on the replaced kaolinite (001) surfaces, the adsorption energies are lower and the adsorption is more stable than adsorption on the ideal kaolinite (001) surface. The optimal adsorption sites are all above the oxygen atoms in the hydroxyl groups, which are parallel to the replaced surfaces and adjacent to the replacement sites.

(2) When the three adsorbates are adsorbed on the kaolinite $Fe(II)_{Al}$-(001) surface, the adsorption stability increases with the number of hydroxyl groups. In contrast, the stability of the adsorption weakened as the number of hydroxyl groups increased when they are adsorbed on the kaolinite Mg_{Al}-(001) surface.

(3) For the adsorption of three adsorbates on the kaolinite $Fe(II)_{Al}$-(001) surface, hydrogen bonding and electrostatic adsorption play a major role. However, when they are adsorbed on the kaolinite Mg_{Al}-(001) surface, the decisive roles are the interaction between the aluminum atoms in the adsorbates and the oxygen atoms on the replaced surface and the electrostatic adsorption between the two.

AUTHOR INFORMATION

Corresponding Author

Fanfei Min − *School of Materials Science and Engineering, Anhui University of Science and Technology, Huainan 232001, China;* orcid.org/0000-0001-9161-745X; Email: ffmin@aust.edu.cn

Authors

Fei Fang − *College of Digital Technology and Engineering, Ningbo University of Finance and Economics, Ningbo 315175, China;* orcid.org/0000-0002-8456-7244

Yan Zheng − *School of Materials Science and Engineering, Anhui University of Science and Technology, Huainan 232001, China;* orcid.org/0000-0001-5176-114X

Jun Chen − *School of Materials Science and Engineering, Anhui University of Science and Technology, Huainan 232001, China;* orcid.org/0000-0001-8104-5419

Chunfu Liu − *School of Materials Science and Engineering, Anhui University of Science and Technology, Huainan 232001, China;* orcid.org/0000-0003-1506-4712

Complete contact information is available at: https://pubs.acs.org/10.1021/acsomega.2c03087

Notes

The authors declare no competing financial interest.

ACKNOWLEDGMENTS

The authors would like to take this opportunity to acknowledge the sponsorship of the Natural Science Foundation of China (Grant Nos. 51874011, 52174233, and 51804009), the Major Project on Natural Science Foundation of Universities in Anhui Province (No. KJ2021ZD0048), and the Key Research and Development Plan Projects in Anhui Province (Grant No. 202004a07020044).

REFERENCES

(1) Liu, D.; Tian, Q.; Yuan, P.; Du, P.; Zhou, J.; Li, Y.; Bu, H.; Zhou, J. Facile sample preparation method allowing TEM characterization of the stacking structures and interlayer spaces of clay minerals. *Appl. Clay Sci.* **2019**, *171*, 1−5.

(2) Presti, D.; Pedone, A.; Mancini, G.; Duce, C.; Tiné, M. R.; Barone, V. Insights into structural and dynamical features of water at halloysite interfaces probed by DFT and classical molecular dynamics simulations. *Phys. Chem. Chem. Phys.* **2016**, *18*, 2164−2174.

(3) Han, Y.; Liu, W.; Chen, J. DFT simulation of the adsorption of sodium silicate species on kaolinite surfaces. *Appl. Surf. Sci.* **2016**, *370*, 403−409.

(4) Zhang, B.; Kang, J.; Kang, T. Effect of water on methane adsorption on the kaolinite (001) surface based on molecular simulations. *Appl. Surf. Sci.* **2018**, *439*, 792−800.

(5) Chen, J.; Min, F.; Liu, L.; Liu, C. Mechanism research on surface hydration of kaolinite, insights from DFT and MD simulations. *Appl. Surf. Sci.* **2019**, *476*, 6−15.

(6) Liu, L.; Min, F.; Chen, J.; Lu, F.; Shen, L. The adsorption of dodecylamine and oleic acid on kaolinite surfaces: Insights from DFT calculation and experimental investigation. *Appl. Surf. Sci.* **2019**, *470*, 27−35.

(7) Ren, B.; Min, F.; Chen, J.; Fang, F.; Liu, C. Adsorption mechanism insights into CPAM structural units on kaolinite surfaces: A DFT simulation. *Appl. Clay Sci.* **2020**, *197*, No. 105719.

(8) Zhang, Z.; Zhou, Q.; Yuan, Z.; Zhao, L.; Dong, J. Adsorption of Mg^{2+} and K^+ on the kaolinite (0 0 1) surface in aqueous system: A combined DFT and AIMD study with an experimental verification. *Appl. Surf. Sci.* **2021**, *538*, No. 148158.

(9) Chen, Z.; Zhao, Y.; Tong, D.; Nie, S.; Wang, Y.; Nie, X.; Jia, Z. A theoretical study of Cs(I) adsorption on kaolinite basal surfaces. *Chem. Phys.* **2022**, *553*, No. 111380.

(10) Zhang, S.; Liu, Q.; Cheng, H.; Zeng, F. Combined experimental and theoretical investigation of interactions between kaolinite inner surface and intercalated dimethyl sulfoxide. *Appl. Surf. Sci.* **2015**, *331*, 234−240.

(11) Alagha, L.; Guo, L.; Ghuzi, M.; Molatlhegi, O.; Xu, Z. Adsorption of hybrid polyacrylamides on anisotropic kaolinite surfaces: Effect of polymer characteristics and solution properties. *Colloids Surf., A* **2016**, *498*, 285−296.

(12) Gui, X.; Xing, Y.; Rong, G.; Cao, Y.; Liu, J. Interaction forces between coal and kaolinite particles measured by atomic force microscopy. *Powder Technol.* **2016**, *301*, 349−355.

(13) Chen, J.; Min, F.; Liu, L.; Liu, C.; Lu, F. Experimental investigation and DFT calculation of different amine/ammonium salts adsorption on kaolinite. *Appl. Surf. Sci.* **2017**, *419*, 241−251.

(14) Ren, B.; Lv, K.; Min, F.; Chen, J.; Liu, C. A new insight into the adsorption behavior of NPAM on kaolinite/water interface: Experimental and theoretical approach. *Fuel* **2021**, *303*, No. 121299.

(15) Qiu, S.; Yan, H.; Qiu, X.; Wu, H.; Zhou, X.; Wu, H.; Li, X.; Qiu, T. Adsorption of La on kaolinite (0 0 1) surface in aqueous system: A combined simulation with an experimental verification. *J. Mol. Liq.* **2022**, *347*, No. 117956.

(16) Bolland, M.; Posner, A.; Quirk, J. Surface charge on kaolinites in aqueous suspension. *Aust. J Soil Res.* **1976**, *14*, No. 197.

(17) Schroth, B. K.; Sposito, G. Surface charge properties of kaolinite. *Clays Clay Miner.* **1997**, *45*, 85−91.

(18) Miranda-Trevino, J. C.; Coles, C. A. Kaolinite properties, structure and influence of metal retention on pH. *Appl. Clay Sci.* **2003**, *23*, 133−139.

(19) Tombácz, E.; Szekeres, M. Surface charge heterogeneity of kaolinite in aqueous suspension in comparison with montmorillonite. *Appl. Clay Sci.* **2006**, *34*, 105−124.

(20) Schofield, R. K.; Samson, H. Flocculation of kaolinite due to the attraction of oppositely charged crystal faces. *Discuss. Faraday Soc.* **1954**, *18*, 135−145.

(21) Malden, P. J.; Meads, R. E. Substitution by Iron in Kaolinite. *Nature* **1967**, *215*, 844−846.

https://doi.org/10.1021/acsomega.2c03087
ACS Omega 2022, 7, 39662−39670

(22) Mestdagh, M. M.; Vielvoye, L.; Herbillon, A. Iron in kaolinite: II. The relationship between kaolinite crystallinity and iron content. *Clay Miner.* **1980**, *15*, 1−13.
(23) Balan, E.; Allard, T.; Boizot, B.; Morin, G.; Muller, J. P. Structural Fe^{3+} in Natural Kaolinites: New Insights from Electron Paramagnetic Resonance Spectra Fitting at X and Q-Band Frequencies. *Clays Clay Miner.* **1999**, *47*, 605−616.
(24) Chi, M.; Eggleton, A.R. Cation exchange capacity of kaolinite. *Clays Clay Miner.* **1999**, *47*, 174−180.
(25) He, M.; Fang, Z.; Zhang, P. Theoretical Studies on Defects of Kaolinite in Clays. *Chin. Phys. Lett.* **2009**, *26*, 262−265.
(26) He, M.; Zhao, J. Effects of Mg, Ca, and Fe(II) Doping on the Kaolinite (001) Surface with H_2O Adsorption. *Clays Clay Miner.* **2012**, *60*, 330−337.
(27) Liu, L.; Min, F.; Chen, J.; Zhang, M.; Lu, F. DFT research on lattice substitution of Fe with different valence states in coal measures kaolinite. *J. China U Min. Technol.* **2019**, *048*, 903−910.
(28) Chen, J.; Min, F.; Liu, L.; Cai, C. Systematic exploration of the interactions between Fe-doped kaolinite and coal based on DFT calculations. *Fuel* **2020**, *266*, No. 117082.
(29) Clark, S. J.; Segall, M. D.; Pickard, C. J.; Hasnip, P. J.; Probert, M. I.; Refson, K.; Payne, M. C. First principles methods using CASTEP. *Z. Kristallogr.-Cryst. Mater.* **2005**, *220*, 567−570.
(30) Fang, F.; Min, F.; Liu, L.; Chen, J.; Ren, B.; Liu, C. Adsorption of Al $(OH)_n^{(3-n)+}$ (n = 2−4) on Kaolinite (001) Surfaces: A DFT study. *Appl. Clay Sci.* **2020**, *187*, No. 105455.
(31) Perdew, J. P.; Burke, K.; Ernzerhof, M. Generalized gradient approximation made simple. *Phys. Rev. Lett.* **1996**, *77*, 3865−3868.
(32) Bučko, T.; Lebègue, S.; Hafner, J.; Angyan, J. G. Tkatchenko-Scheffler van der Waals correction method with and without self-consistent screening applied to solids. *Phys. Rev. B* **2013**, *87*, No. 064110.
(33) Chen, J. *Principles of the Flotation of Sulphide Minerals Bearing Lattice Defects*; Central South University Press: Changsha, 2012; pp 51−54.
(34) Kremleva, A.; Krüger, S.; Rösch, N. Density Functional Model Studies of Uranyl Adsorption on (001) Surfaces of Kaolinite. *Langmuir* **2008**, *24*, 9515−9524.
(35) Bish, D. L. Rietveld Refinement of the Kaolinite Structure at 1.5 K. *Clays Clay Miner.* **1993**, *41*, 738−744.
(36) Fukui, K. The path of chemical reactions - the IRC approach. *Acc. Chem. Res.* **1981**, *14*, 363−368.
(37) Fukui, K. Role of Frontier Orbitals in Chemical Reactions. *Science* **1982**, *218*, 747−754.
(38) Chen, J. *The Solide Physics of Sulphide Minerals Flotation*; Central South University Press, 2015.
(39) Chen, J.; Li, Y. Orbital symmetry matching study on the interactions of flotation reagents with mineral surfaces. *Miner. Eng.* **2022**, *179*, No. 107469.

https://doi.org/10.1021/acsomega.2c03087
ACS Omega 2022, 7, 39662−39670